Dynamic Light Scattering of Short Au Rods with Low Aspect Ratios

Jessica Rodríguez-Fernández, Jorge Pérez−Juste, Luis M. Liz−Marzán, and Peter R. Lang*,†

Departamento de Química Física and Unidad Asociada CSIC, Universidade de Vigo, 36310, Vigo, Spain, and Forschungszentrum Jülich, Institut für Festkörperforschung, Weiche Materie, D-52425 Jülich, Germany

Received: October 27, 2006; In Final Form: February 1, 2007

The translational and rotational diffusion of a series of gold nanorods with low aspect ratios was investigated by dynamic light scattering (DLS). It is shown that the translational and rotational diffusion coefficients can be determined because the particle shape causes an anisotropy of the polarizability. This gives rise to two clearly distinguishable relaxation modes in the time correlation function of the scattered light. The particle length and aspect ratio were determined independently by transmission electron microscopy (TEM). Using a hydrodynamic model, these geometrical parameters were converted to diffusion constants, which agree well with the values determined by DLS. Additionally, it is possible to obtain an estimate of the particles' aspect ratio from the amplitude ratio of the two relaxation modes.

Introduction

Metal nanoparticles have received a great deal of attention since the early times of colloid science, when Michael Faraday first observed the range of different colors that gold colloids display as a function of size.[1] Since then, a plethora of studies have dealt with the production and characterization of noble metal colloids in a wide range of sizes[2−4] and for a variety of applications, including catalysis,[5] biolabeling,[6] biosensing,[7] and optical switches,[8] among others. Only recently, variations in nanoparticle shape have been recognized as having a strong impact on their properties, which has motivated the development of synthetic methods for the preparation of particles with various geometries, such as rods,[9−13] wires,[14−16] prisms,[17−21] cubes,[22−24] and other polyhedrons.[25,26] Most of these methods are based on wet chemistry reactions involving the reduction of metal salts and the adsorption of surfactants or other molecules, generally known as capping agents. The mechanisms directing the growth of particles with a particular geometry are still a matter of debate for most systems, but what is general is that they involve the growth of pre-existing nuclei in solution and this leads to a random process that implies that all particles are different, even in the most monodisperse samples. The characterization of the dimensions for such a variety of shapes is usually carried out using electron microscopy (EM), which implies the measurement of a large number (typically >100) of particles followed by averaging. This provides values for average dimensions and polydispersity (usually as standard deviation) but still is only representative of a limited population within the sample and therefore may not provide the real size distribution of the whole sample. Additionally, EM measurements are carried out on dry samples, under vacuum and irradiating the specimen with high-energy electron beams, which very likely affect the morphology and dimensions of the particles. We have been working on gold nanorods for several years now, with the objective to understand the mechanism underlying their formation[13,27,28] as well as to understand and manipulate their extremely interesting, surface plasmon-related optical properties.[29−31]

In this context, we have identified the need to apply alternative characterization techniques that overcome the mentioned drawbacks, that is, techniques that probe a larger amount of particles, do not require solvent evaporation, and do not modify the particles themselves. Such requirements are fulfilled by scattering methods, which have been used widely and successfully for other colloidal systems. Among the various scattering techniques, light scattering is the one requiring a simpler setup, and therefore it is available at many laboratories. However, its use to characterize metal colloids in general and gold nanorods in particular has not been very popular because of heating problems derived from absorption of the laser beam, limited applicability of the Rayleigh−Gans−Debye approximation, small particle sizes, and because models to analyze data for nonspherical particles seemed complicated. In the literature dealing with dynamic light scattering of rodlike particles, very often the limiting case of rods with negligible anisotropy of the polarizability is considered, where different scenarios have to be applied depending on the rod length, L. For systems where the product of the scattering vector magnitude and rod length $QL \lesssim 5$, a single−exponential decay of the correlation function of the scattered intensity $g_2(t)$ (ITCF) is expected, provided the rods are fairly monodisperse in length. In the case where $QL > 10$, additional relaxation modes are observed in the correlation function. However, these cases are not relevant for our systems, because (i) the anisotropy of the polarizability of gold nanorods is not negligible, especially for particles with low aspect ratios,[33] and (ii) the length of the rods in our case lies typically in the 50 nm range, that is, $QL \lesssim 1$. Nevertheless, we clearly observed two relaxation modes in the ITCF. To our knowledge, two relaxation modes in the correlation function from rods smaller than 50 nm in length have been reported only once,[34] in a fluorescence correlation spectroscopy (FCS) experiment. However, in that case the relaxation times of the relaxation mode that is ascribed to the translational diffusion is larger by 2 orders of magnitude than those in our case, even though the particles are of comparable size. We therefore conjecture that long-time diffusion has been observed in that case, while we are

* Corresponding author. E-mail: p.lang@fz-juelich.de.
† Forschungszentrum Jülich, Institut für Festkörperforschung.

10.1021/jp067049x CCC: $37.00
Published on Web 03/13/2007

investigating short-time Brownian dynamics. Thus, the unexpected appearance of two relaxation modes requires a thorough analysis.

An expression for the time autocorrelation function for the scattered field can be extracted from the seminal work by Pecora,[35] who showed that the spectral density of the scattered light can be expressed as the sum of an isotropic and anisotropic contribution. Fourier transforming the spectral density gives the time dependence of the field autocorrelation function, from which $g_2(t)$ can be calculated using the Siegert relation. By nonlinear least-squares fitting of this expression to our experimental data, we determined the averaged translational, $\bar{D}$, and the rotational, D_r, diffusion coefficient of the Au rods. Furthermore, we could obtain an estimate of the particle aspect ratio from the relative amplitudes of the ITCF. The paper is structured as follows. We describe the Au rod synthesis, as well as the data acquisition and analysis procedures in the experimental section, while the results from dynamic light scattering are discussed and compared to transmission electron microscopy (TEM) data in the results and discussion section. Finally, we append a brief derivation of the expression for the ITCF for the non-expert reader.

Experimental

Synthesis and Characterization of Au Rods. A series of Au nanorod samples (labeled as Au-1 to Au-5) with different aspect ratios were prepared through a seeding growth method first reported by Nikoobakht and El-Sayed[12] growing CTAB stabilized Au nanoparticle seeds (<3 nm) by reduction of $HAuCl_4$ with ascorbic acid in the presence of a BDAC/CTAB mixture (in a 2.7 ratio) and a small amount of $AgNO_3$. The aspect ratio was varied through the amount of seed solution added (increasing from Au-1 to Au-5). Sample Au-6 was synthesized according to the modification of the seeding growth method reported by Liu and Guyot-Sionnest,[32] where the reduction of $HAuCl_4$ with ascorbic acid on the preformed Au seeds in CTAB is carried out in the presence of HCl, to adjust the pH between 2 and 3. Tetrachloroauric acid ($HAuCl_4 \cdot 3H_2O$), cetyltrimethylammonium bromide (CTAB), benzyldimethylammonium chloride (BDAC), ascorbic acid, sodium borohydride ($NaBH_4$), $AgNO_3$, and hydrochloric acid (HCl) were purchased from Aldrich and used as received. Milli-Q water with a resistivity higher than 18.2 MΩ·cm was used in all of the preparations.

Optical characterization was carried out by UV−visible−NIR spectroscopy with a Cary 5000 UV−vis−NIR spectrophotometer, using 10-mm-path-length quartz cuvettes. Transmission electron microscopy (TEM) images from all samples were obtained with a JEOL JEM 1010 transmission electron microscope operating at an acceleration voltage of 100 kV. In the series from Au−1 through Au−5, the average aspect ratio of the particles was found to increase from 4.2 to 5.5, as expected from the synthesis conditions. For sample Au-6 the aspect ratio is 4.2 (see Table 1).

Dynamic Light Scattering. Sample solutions for light scattering were prepared from the original solution by repeated dilution steps with water, until the transmission of the solution and that of water could not be distinguished any more at a wavelength of $\lambda_0 = 647$ nm. We further checked that additional dilution by a factor of 2 did not change the relaxation times of the time autocorrelation functions. In this case, we may consider the solutions as infinitely dilute.

Time autocorrelation functions of the scattered intensity $g_2(Q, t)$ were recorded with a standard DLS apparatus equipped with a Kr ion laser ($\lambda_0 = 647$ nm) as a light source. The scattering angle, θ, was varied from 40° to 130° in steps of 10°; accordingly, the scattering vector $Q = 4\pi n_s \sin(\theta/2)/\lambda_0$ covered a range of 8.835×10^{-3} nm $< Q < 2.34 \times 10^{-2}$ nm. The polarization state of incident and scattered light was controlled with a $\lambda/2$ plate and a polarizer in the primary beam and an analyzer (all polarizing optics from Bernhard Halle Nachfl, Berlin Germany) in the scattered beam. The scattered light was collected with a monomode optical fiber (OZ-Optics, Ottawa, Canada) and detected with a SOSIP dual photomultiplier unit by ALV Laserverstriebsgesellschaft mbH, Langen, Germany. The TTL output of the avalanche diode was processed in the cross-correlation mode of a multiple tau correlator, ALV-5000. The shortest delay time, which is reliably accessible with this detector−correlator combination, is ~100 ns. For each sample, a complete angular set of correlation functions was recorded in both vertical−vertical (VV) and vertical−horizontal (VH) geometry.

TABLE 1: Mean Translational, $\bar{D}$, and Rotational, D_r, Diffusion Coefficients Measured by DLS of Gold Rods in Suspension, and Rod Lengths L as Well as Aspect Ratios, L/d_{cs} from TEM

sample	$\bar{D}$ (nm²/ms)	D_r (ms⁻¹)	L (nm)	L/d_{cs}
Au-1	12 200 ± 200	23.2 ± 0.6	45.9 ± 6.3	4.2 ± 1.1
Au-2	14 100 ± 400	29.7 ± 0.3	38.2 ± 5.9	4.4 ± 0.9
Au-3	15 200 ± 600	36.5 ± 1.2	38.4 ± 5.0	4.6 ± 1.0
Au-4	16 300 ± 600	47.3 ± 0.9	37.5 ± 5.4	5.2 ± 1.1
Au-5	19 000 ± 500	52.6 ± 0.3	37.3 ± 5.7	5.5 ± 1.2
Au-6	7100 ± 400	8.3 ± 0.7	60.6 ± 10.4	4.2 ± 0.8

Data Analysis. For the particular case of small particles with cylindrical shape and non-negligible anisotropy of the polarizability, expressions for the normalized intensity autocorrelation functions measured in the VH and VV geometry are given by

$$g_2^{VV}(Q, t) - 1 = \beta[A^2 \exp\{-\Gamma t\} + 2AB \exp\{-(\Gamma + \Delta/2)t\} + B^2 \exp\{-(\Gamma + \Delta)t\}] \quad (1)$$

$$g_2^{VH}(Q, t) - 1 = \beta' \exp\{-(\Gamma + \Delta)t\} \quad (2)$$

respectively. Here $\Gamma = 2\bar{D}Q^2$ and $\Delta = 12D_r$, while $A + B = 1$ (see the appendix for details). The parameters β and β' describe the nonideal dynamical contrast of the light scattering setup and are slightly less than unity. According to eqs 1 and 2, the standard procedure to determine $\bar{D}$ and D_r is to plot the relaxation rate of $g_2^{VH}(t) - 1$ versus Q^2. The intercept of the resulting linear relation is $12D_r$ and the slope is $2\bar{D}$. Furthermore, a plot of the relaxation rate of $g_2^{VV}(t \gg 1/6D_r) - 1$ gives a linear relation with a slope of $2\bar{D}$ and zero intercept. We decided not to use this procedure for three reasons. First, the choice of the threshold $t \gg 1/6D_r$ could not be determined unambiguously from our data. Second, as will turn out, the relaxation rate of $g_2^{VH}(t) - 1$ does not depend significantly on the scattering vector. This implies that $6D_r \gg \bar{D}$ and that $\bar{D}$ cannot be determined with high reliabilty from either of the two mentioned possibilities. Third, the determination of the relaxation rates requires some kind of least-squares fitting in any case. We therefore chose to nonlinear least-squares fit the entire ITCFs by eqs 1 and 2 to determine D_r and $\bar{D}$. This has the further advantage that the amplitudes of the two relaxation modes can also be determined, which carry information on the aspect ratio of the particles. To achieve the highest possible reliability of the best fitting parameters, we applied a global fitting algorithm, in which we analyzed the complete set of correlation functions

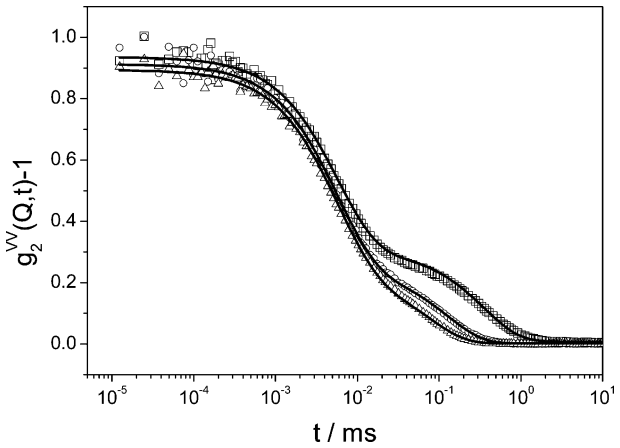

Figure 1. ITCF from sample Au-1 recorded in the VV geometry. Different symbols refer to different scattering angles. For the sake of clarity, only 3 out of 10 curves are displayed, i.e., 40° (□), 90° (○), and 130° (△). Full lines are nonlinear least-squares fits according to eq 1.

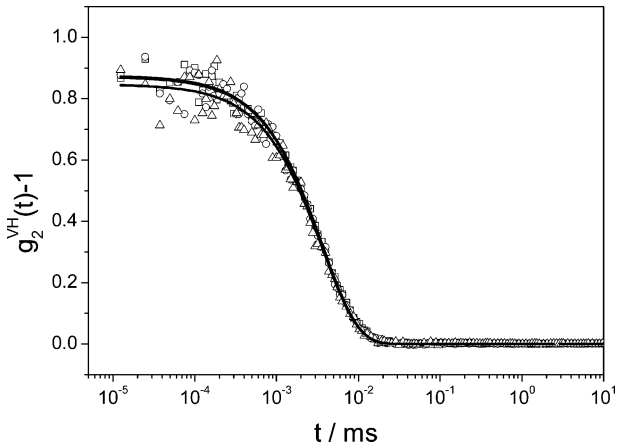

Figure 2. ITCF from sample Au-1 recorded in the VH geometry. Different symbols refer to different scattering angles. For the sake of clarity, only 3 out of 10 curves are displayed, i.e., 40° (□), 90° (○), and 130° (△). Full lines are nonlinear least-squares fits according to eq 2.

obtained from one sample simultaneously. In this procedure A, $\bar{D}$, and D_r were treated as global parameters, while β and β' were allowed to vary between different correlation functions.

Results and Discussion

The choice of samples for the measurements was based on a compromise among various parameters. First, we intended to achieve a reasonably wide range of aspect ratios, and whenever possible of particle size. However, to avoid excessive absorption of the incident laser beam (647 nm), which would lead to significant local heating, the corresponding transverse and longitudinal surface plasmon absorption bands should be located below and above this wavelength, respectively. Another constraint was the need for the highest monodispersity achievable in practice, which is mainly restricted to aspect ratios below 6. Because low aspect ratios would involve high absorption at the wavelength of interest and high aspect ratios lead to high polydispersity, we decided to concentrate on a relatively narrow range of aspect ratios between 4.2 and 5.5. As described in Table 1, for aspect ratios between 4.4 and 5.5, the nanorod average length was maintained approximately constant, with a systematic variation of the width, while for aspect ratio 4.2, two relatively different dimensions were selected. The UV−vis−NIR spectra for all samples are shown in the Supporting Information, together with representative TEM images.

Intensity autocorrelation functions (ITCF) obtained from sample Au-1 recorded in VV geometry are displayed in Figure 1. For clarity, we have plotted only the curves from three different scattering angles, namely, 40°, 90°, and 130°. It can be clearly seen that at all different angles there are two relaxation modes, one of which becomes faster with increasing θ, and one which is virtually independent of the scattering angle. Similarly, the relaxation times of the ITCF recorded in VH geometry do not change with scattering angle. This is shown for sample Au-1 in Figure 2. This behavior is not expected at first glance from eqs 1 and 2 because all exponentials in these equations have relaxation rates that are linearly proportional to Q^2. Alternatively, if $\bar{D}Q^2 \ll D_r$ then only the first term of eq 1 depends significantly on the scattering angle. This means that the slow relaxation mode in the VV correlation functions is related to the translational diffusion of the rods alone while the fast mode and the relaxation rates of the VH correlation functions are dominated by rotational diffusion. Global fitting of the experimental ITCF as described in the experimental section yielded

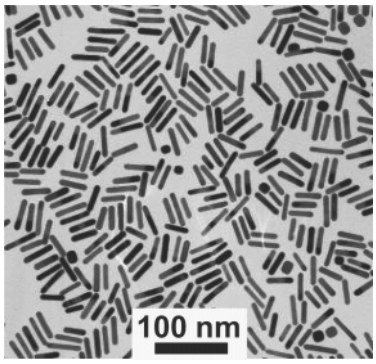

Figure 3. TEM micrograph of sample Au-4.

the parameters listed in Table 1. In this table we also list the geometrical particle parameters, L and L/d_{cs}, obtained from the analysis of TEM micrographs. The deviations listed together with the data are reliability intervals from the fitting routine in case of the diffusion coefficients. In the case of the parameters from TEM, they represent the standard deviation of the distribution of the corresponding parameter. As a representative example, we show a TEM picture in Figure 3.

This micrograph shows that the rods have relatively narrow distribution both in length and in aspect ratio, which is confirmed by the standard deviations of the corresponding distributions, which are in the range of 15% for the length and about 10% for the aspect ratio. We also observe a small number of cubes, which is a general finding in these samples. However, their relative amount is very low and thus they are not expected to contribute significantly to the global scattering of the sample. Therefore, we will consider the rods to be monodisperse in the following discussion. A first approximation for the relation between geometrical parameters and diffusion constants of colloidal rods has been given by Brørsma,[36,37] which, however, is sufficiently accurate only for rods with $\ln(L/d_{cs}) > 2$. Because this requirement is not fulfilled for our Au rods, we chose to apply the expression by Ortega and de la Torre[38]

$$\bar{D} = \frac{k_B T(\ln(L/d_{cs}) + \bar{C})}{3\pi\eta L}$$

$$D_r = \frac{3k_B T(\ln(L/d_{cs}) + C_r)}{\pi\eta L^3} \qquad (3)$$

TABLE 2: Mean Translational, $\bar{D}$, and Rotational, D_r, Diffusion Coefficients Measured by DLS, and Corresponding Values, $\bar{D}^*$ and D_r^*, Calculated by Using Equations 3 and 4 and the Geometrical Parameter Listed in Table 1[a]

sample	$\bar{D}$ (nm^2/ms)	D_r (ms^{-1})	$\bar{D}^*$ (nm^2/ms)	D_r^* (ms^{-1})
Au-1	12 200	23.2	13 900	19.4
Au-2	14 100	29.7	16 000	30.1
Au-3	15 200	36.5	16 200	30.4
Au-4	16 300	47.3	17 000	34.2
Au-5	19 000	52.6	17 300	35.4
Au-6	7100	8.3	11 400	10.1

[a] In addition, a stabilizing surfactant layer of 4 nm thickness was accounted for.

Here $\bar{C}$ and C_r are second-order polynomials in d_{cs}/L, the coefficients of which have been determined by fitting of numerical data.

$$\bar{C} = 0.312 + 0.565\frac{d_{cs}}{L} - 0.100\left(\frac{d_{cs}}{L}\right)^2$$

$$C_r = 0.662 + 0.917\frac{d_{cs}}{L} - 0.05\left(\frac{d_{cs}}{L}\right)^2 \quad (4)$$

These equations apply to our particles because they were derived for the range of $2 < L/d_{cs} < 20$. In Table 2, we compare the diffusion coefficients measured by DLS with those calculated with eqs 3 and 4. Reasonable agreement between the experimental and the calculated values could only be achieved by considering a double layer of CTAB around the rods, which stabilizes the particles by exposing the charged ammonium groups to the polar solvent.[39,40] The thickness of this bilayer was estimated to be ca. 4 nm according to the standard rule of thumb for the contour length of an alkane chain, that is, $l_c = n \times 0.126 + 0.154$ nm,[41] where n is the number of carbon atoms in the chain. A similar effect was observed by van der Zande et al.[42] for long gold rods (typically $L > 200$ nm and $L/d_{cs} > 10$), which were sterically stabilized by an adsorbed polymer layer. These authors found that the translational diffusion coefficients were up to a factor of 4 smaller than those expected from the particles' geometrical parameters. For the rotational diffusion coefficient, the discrepancy could even amount to almost an order of magnitude. This discrepancy was assigned to the stabilizing polymer layer, which in this case had a thickness comparable to the particles cross-sectional diameter.

In the present study, we find agreement between the calculated and experimental values within less than 20% for the rotational diffusion coefficient of the particles with an aspect ratio smaller than 5. Only for the two samples with the largest aspect ratios the discrepancy is ca. 30%. In the case of $\bar{D}$, the agreement is better than 15% in most cases with a slight tendency to decrease with increasing aspect ratio of the rods. This is probably due to the fact that the theory by Ortega and Garcia de la Torre was devised for cylinders with flat base areas while our gold rods are more of spherocylindrical shape, as can be seen from Figure 3. Intuitively, one would expect this effect to become smaller with increasing aspect ratio of the rods.

As mentioned above, it is possible to obtain information on the particle aspect ratio from the ratio of the relative amplitudes A/B of the two relaxation modes measured in VV geometry. This will be discussed in detail in the following. According to Pecora,[35] the ratio of the amplitudes is related to the components of the polarizability tensor by

$$\frac{A}{B} = \frac{5}{4}\frac{\alpha_I^2}{\langle(\alpha_\perp - \alpha_{||})^2\rangle}$$

where || denotes the direction parallel to the rod's long axis and $\perp$ the direction normal to it. If the particle size is small compared to the wavelength, the dipole approximation applies.[43] In this case, Rayleigh's theory[44] for the polarizability of ellipsoids is commonly used to estimate the polarizability of the rods.[45] Applying this approximation is necessary because there is no theoretical expression for rods available. According to Rayleigh, the polarizability of an ellipsoid in the direction of one of the symmetry axes is

$$\alpha_j = V\frac{\epsilon - \epsilon_m}{\epsilon_m + L_j(\epsilon - \epsilon_m)} \quad (5)$$

where V is the volume of the ellipsoid, $\epsilon = \epsilon' + \imath\epsilon''$ is the complex dielectric function of the ellipsoid material at a given wavelength, ϵ_m is the dielectric constant of the solvent, and $j =$ || or $\perp$ denotes the axis of the ellipsoid. Note that the value of the dielectric function is the same for all axes and any anisotropy of the polarization is a mere geometrical effect that is due to the factors

$$L_{||} = \frac{1-e^2}{e^2}\left(\frac{1}{2e}\ln\frac{1+e}{1-e} - 1\right) \quad (6)$$

$$L_\perp = \frac{1 - L_{||}}{2} \quad (7)$$

for an ellipsoid of revolution, for which the two normal axes are equally long. The eccentricity of the ellipsoid is $e = \sqrt{(1-(b/a)^2)}$ where a is the length of the rotation axis and b the length of the axis normal to that. To apply this formalism to approximate the properties of rods b/a has to be replaced by d_{cs}/L.

Thus, the amplitude ratio of the ITCF can be related directly to the aspect ratio and the dielectric function of the particle. After some straight-forward algebra, one obtains

$$\frac{A}{B} = \frac{5}{4}\frac{4\mathcal{M}_\perp + 2\mathcal{N}\mathcal{M}_{||}\mathcal{M}_\perp + \mathcal{M}_{||}}{\langle\mathcal{M}_\perp - \mathcal{N} + \mathcal{M}_{||}\rangle} \quad (8)$$

Here $\mathcal{M}_j = [(\epsilon_m + L_j\epsilon')^2 + L_j^2\epsilon''^2]^{-1}$ and $\mathcal{N} = 2[\epsilon_m^2 + \epsilon_m\epsilon'(L_\perp + L_{||}) + L_\perp L_{||}(\epsilon'^2 + \epsilon''^2)]$. With this expression, we calculated the dependence of A/B on the particle aspect ratio, which is shown in Figure 4, together with the experimental data for A/B. For the dielectric function of gold at $\lambda_0 = 647$ nm we used $\epsilon' = -12.789$ and $\epsilon'' = 1.116$,[46] and for the solvent we took the value of water $\epsilon_m = n^2 = 1.772$. We find good qualitative agreement between the calculated curve and the experimental data points. Generally, the theoretical curve is lying below the data points with an increasing deviation toward smaller aspect ratios. This is probably due to the approximation of the rods' polarizabilty, by that of an ellipsoid. Because the anisotropy of the polarizabilty is only due to the particle shape, this approximation is expected to hold better for larger aspect ratios. Furthermore, the single data point that is lying below the theoretical curve corresponds to sample Au-6, which is significantly longer than the others. This might lead to reduction of A due to the influence of the particle form factor $P(Q)$.

Generally, the above calculations show that the amplitude of the relaxation mode, which depends on the translational and

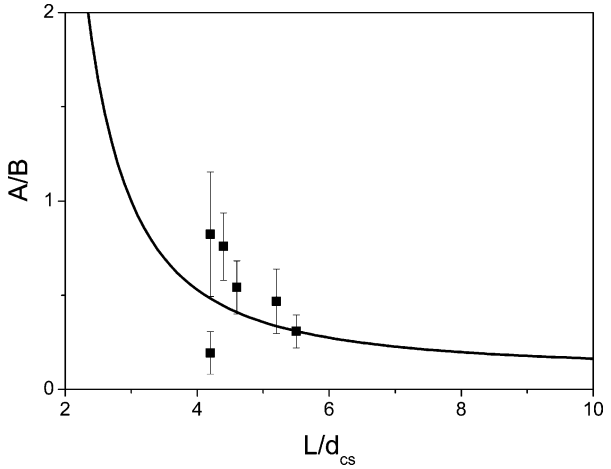

Figure 4. Amplitude ratio of the relaxation modes in $g_2(t) - 1$ vs aspect ratio. Symbols are experimental points as determined by DLS and TEM. The full line was calculated using eq 8.

rotational diffusion coefficients, that is, *B* becomes increasingly dominating with respect to *A*, if the particle aspect ratio exceeds a value of 10. This is obviously the reason that in the pioneering work by van der Zande et al.[42] on dynamic light scattering of gold rods a single relaxation process of the ITCF was observed. These authors had investigated only samples with $L/d_{cs} > 12$ with dynamic light scattering. They refrained from DLS measurements of the rods with smaller aspect ratios because of the high polydispersity of their samples.[47]

Conclusions

The autocorrelation function of the scattered intensity recorded in VV geometry from gold rods with small aspect ratios shows two distinct relaxation processes. Applying Pecora's expression for the correlation function, we determined the translational and rotational diffusion coefficients as well as the amplitudes of the individual relaxation modes. The diffusion coefficients are in good agreement with the values calculated from the geometrical parameters of the rods, if the thickness of the stabilizing surfactant bilayer is taken into account. Furthermore, we presented a path to estimate the aspect ratio of the particles from the ratio of the relative amplitudes of the correlation function.

Acknowledgment. Part of this work was supported by the European Network of Excellence *SoftComp*, which is gratefully acknowledged. J.R.-F. acknowledges the Spanish Ministerio de Educación y Ciencia for granting an F.P.U. fellowship, and L.M.L.M. for funding through grant No. MAT2004-02991. We thank Jan Dhont for helpful discussions.

Appendix

Time Autocorrelation Function, $g_1(t)$, of the Scattered Field. In ref 35, Pecora showed that the spectral density of scattered light can be written as the sum of an isotropic and an anisotropic contribution

$$I(Q, \omega) = I_{iso}(Q, \omega) + I_{aniso}(Q, \omega) \tag{9}$$

with

$$I_{iso}(Q, \omega) = \frac{\rho}{2\pi} K^2 \cos^2(\phi) \sin^2(\theta)\, \alpha_I{}^2 P(Q)\, S_{iso}(Q, \omega) \tag{10}$$

and

$$I_{aniso}(Q, \omega) = \frac{\rho}{30\pi} K^2 (3 + \cos^2(\phi) \sin{}^2(\theta))\, S_{aniso}(Q, \omega) \tag{11}$$

where ρ is the particle number density, K is an optical contrast factor, and $\alpha_I = (2\alpha_\perp + \alpha_{||})/3$. The angle between the wave vector of the scattered light and the polarization vector of the incident light is denoted θ, while ϕ is the angle between the polarization vector of the scattered light and the plane span by the wave vector of the scattered light and the polarization vector of the incident light. Thus, in VV geometry $\cos^2(\phi)\sin^2(\theta) = 1$, and $\cos^2(\phi)\sin^2(\theta) = 0$ in VH geometry. The isotropic contribution to the dynamic structure factor is given by the Lorentzian

$$S_{iso}(Q, \omega) = \frac{2Q^2\bar{D}}{\omega^2 + (Q^2\bar{D})^2} \tag{12}$$

while the anisotropic contribution consists of a sum of five Lorentzians. For the particularly simple case of particles with cylindrical symmetry, the latter reduces to

$$S_{aniso}(Q, \omega) = \frac{\langle(\alpha_\perp - \alpha_{||})^2\rangle}{3} \frac{2(Q^2\bar{D} + 6D_r)}{\omega^2 + (Q^2\bar{D} + 6D_r)^2} \tag{13}$$

According to the Wiener−Khinchin theorem, the time autocorrelation function of the scattered light is related by a Fourier transformation to the spectral density; thus

$$g_1(t) = \tilde{S}_{iso}(Q, t) + \tilde{S}_{aniso}(Q, t) \tag{14}$$

Consequently, we get for the normalized field autocorrelation function in VV geometry

$$\hat{g}_1^{VV}(t) = A \exp\{-\bar{D}Q^2 t\} + B \exp\{-(\bar{D}Q^2 + 6D_r)\} \tag{15}$$

with $A = \alpha_I^2/(\alpha_I^2 + \langle(\alpha_\perp - \alpha_{||})^2\rangle)$ and $B = 4/15\langle(\alpha_\perp - \alpha_{||})^2\rangle/(\alpha_I^2 + \langle(\alpha_\perp - \alpha_{||})^2\rangle)$. The corresponding expression for VH geometry is

$$\hat{g}_1^{VH}(t) = \exp\{-(\bar{D}Q^2 + 6D_r)\} \tag{16}$$

Applying the Siegert−relation gives the final expressions of eqs 1 and 2, which we used as model functions for the analysis of our experimental data.

Supporting Information Available: The UV−vis−NIR spectra and representative TEM micrographs for all samples. This material is available free of charge via the Internet at http://pubs.acs.org.

References and Notes

(1) Faraday, M. *Philos. Trans. R. Soc. London* **1857**, *147*, 145.
(2) Frens, G. *Nature* **1973**, *241*, 20.
(3) Rodríguez-Fernández, J.; Pérez-Juste, J.; García de Abajo, F. J.; Liz-Marzán, L. M. *Langmuir* **2006**, *22*, 7007.
(4) Evanoff, D. D., Jr.; Chumanov, G. *J. Phys. Chem. B* **2004**, *108*, 13948.
(5) Toshima, N. *Metal Nanoparticles for Catalysis* in *Nanoscale Materials*; Kluwer Academic Publishers: Boston, MA, 2003.
(6) Gittins, D. I.; Caruso, F. *Chem. Phys. Chem.* **2002**, *3*, 110.
(7) Lee, K.-S.; El-Sayed, M. A. *J. Phys. Chem. B* **2006**, *110*, 19220.
(8) Hu, M.-S.; Chen, H.-L.; Shen, C.-H.; Hong, L.-S.; Huang, B.-R.; Chen, K.-H.; Chen, L.-C. *Nat. Mater.* **2006**, *5*, 102.
(9) van der Zande, B. M. I.; Boehmer, M. R.; Fokkink, L. G. J.; Schoenenberger, C. *J. Phys. Chem. B* **1997**, *101*, 852.

(10) Chang, S.-S.; Shih, C.-W.; Chen, C.-D.; Lai, W.-C.; Wang, C. R. C. *Langmuir* **1999**, *15*, 701.
(11) Busbee, B. D.; Obare, S. O.; Murphy, C. *J. Adv. Mater.* **2003**, *15*, 414.
(12) Nikoobakht, B.; El-Sayed, M. A. *Chem. Mater.* **2003**, *15*, 1957.
(13) Pérez-Juste, J.; Liz-Marzán, L. M.; Carnie, S.; Chan, D. Y. C.; Mulvaney, P. *Adv. Funct. Mater.* **2004**, *14*, 571.
(14) Sun, Y.; Gates, B.; Mayers, B.; Xia, Y. *Nano Lett.* **2002**, *2*, 165.
(15) Sun, Y.; Yin, Y.; Mayers, B. T.; Herricks, T.; Xia, Y. *Chem. Mater.* **2002**, *714*, 4736.
(16) Vasilev, K.; Zhu, T.; Wilms, M.; Gillies, G.; Lieberwirth, I.; Mittler, S.; Knoll, W; Kreiter, M. *Langmuir* **2005**, *21*, 12399.
(17) Jin, R.; Cao, Y.; Mirkin, C. A.; Kelly, K. L.; Schatz, G. C.; Zheng, J. G. *Science* **2001**, *294*, 1901.
(18) Pastoriza-Santos, I.; Liz-Marzán, L. M. *Nano Lett.* **2002**, *2*, 903.
(19) Sun, Y.; Xia, Y. *Adv. Mater.* **2003**, *15*, 695.
(20) Millstone, J. E.; Park, S.; Shuford, K. L.; Qin, L.; Schatz, G. C.; Mirkin, C. A. *J. Am. Chem. Soc.* **2005**, *127*, 5312.
(21) Bastys, V.; Pastoriza-Santos, I.; Rodríguez-González, B.; Vaisnoras, R.; Liz-Marzán, L. M. *Adv. Funct. Mater.* **2006**, *16*, 766.
(22) Sun, Y.; Xia, Y. *Science* **2002**, *298*, 2176.
(23) Kim, F.; Connor, S.; Song, H.; Kuykendall, T.; Yang, P. *Angew. Chem., Int. Ed.* **2004**, *43*, 3673.
(24) Im, S. H.; Lee, Y. T.; Wiley, B.; Xia, Y. *Angew. Chem., Int. Ed.* **2005**, *44*, 2154.
(25) Wiley, B. J.; Xiong, Y.; Li, Z.-Y.; Yin, Y.; Xia, Y. *Nano Lett.* **2006**, *6*, 765.
(26) Sánchez-Iglesias, A.; Pastoriza-Santos, I.; Pérez-Juste, J.; Rodríguez-González, B.; García de Abajo, F. J.; Liz-Marzán, L. M. *Adv. Mater.* **2006**, *18*, 2529.
(27) Rodríguez-Fernández, J.; Pérez-Juste, J.; Mulvaney, P.; Liz-Marzán, L. M. *J. Phys. Chem. B* **2005**, *109*, 14257.
(28) Grzelczak, M.; Pérez-Juste, J.; Rodríguez-González, B.; Liz-Marzán, L. M. *J. Mater. Chem.* **2006**, *16*, 3946.
(29) Pérez-Juste, J.; Rodríguez-González, B.; Mulvaney, P.; Liz-Marzán, L. M. *Adv. Funct. Mater.* **2005**, *15*, 1065.
(30) Correa-Duarte, M. A.; Pérez-Juste, J.; Sánchez-Iglesias, A.; Giersig, M.; Liz-Marzán, L. M. *Angew. Chem., Int. Ed.* **2005**, *44*, 4375.
(31) Pastoriza-Santos, I.; Pérez-Juste, J.; Liz-Marzán, L. M. *Chem. Mater.* **2006**, *18*, 2465.
(32) Liu, M.; Guyot-Sionnest, P. *J. Phys. Chem. B* **2005**, *109*, 22192.
(33) Khlebtsov, N. G.; Melnikov, A. G.; Bogatyrev, V. A.; Dykman, L. A.; Alekseeva, A. V.; Trachuk, L. A.; Khlebtsov, B. N. J. *Phys. Chem. B* **2005**, *109*, 13578.
(34) Pelton, M.; Liu, M; Kim, H. Y.; Smith, G.; Guyot−Sionnest, P.; Scherer, N. F. *Opt. Lett.* **2006**, *31*, 2075.
(35) Pecora, R. *J. Chem. Phys.* **1968**, *49*, 1036.
(36) Broersma, S. *J. Chem. Phys.* **1960**, *32*, 1626.
(37) Broersma, S. *J. Chem. Phys.* **1960**, *32*, 1632.
(38) Ortega, A.; Garcia de la Torre, J. *J. Chem. Phys.* **2003**, *119*, 9914.
(39) Gao, J.; Bender, C. M.; Murphy, C. J. *Langmuir* **2003**, *19*, 9065.
(40) Nikoobakht, B.; El-Sayed, M. A. *Langmuir* **2001**, *17*, 6368.
(41) Tanford, C. *The Hydrophobic Effect*; Wiley: New York, 1973.
(42) van der Zande, B. M. I.; Dhont, J. K. G.; Böhmer, M. R.; Philipse, A. P. *Langmuir* **2000**, *16*, 459.
(43) Mie, G. *Ann. Phys.* **1908**, *25*, 377.
(44) Lord Rayleigh *Philos. Mag.* **1897**, *44*, 28.
(45) Pérez-Juste, J.; Pastoriza-Santos, I.; Liz-Marzan, L. M.; Mulvany, P. *Coord. Chem. Rev.* **2005**, *249*, 1870.
(46) Johnson, P. B.; Christy, R. W. *Phys. Rev. B* **1972**, *8*, 4370.
(47) Dhont, J. K. G. Personal communication.